IEEE Access
Multidisciplinary | Rapid Review | Open Access Journal

Received July 27, 2019, accepted August 13, 2019, date of publication August 28, 2019, date of current version September 11, 2019.

Digital Object Identifier 10.1109/ACCESS.2019.2937938

Spatial Power Combining of DSSS Signals From a Sparse Array

XIAOFENG OUYANG, FANGLING ZENG, DAQIAN LV, AND WENHAO WANG
School of Electronic Engineering, National University of Defense Technology, Hefei 230037, China

Corresponding author: Xiaofeng Ouyang (xfouyang@sina.com)

This work was supported in part by the 13th Five-year Plan Equipment Pre-Research Fund of China under Grant 61403110306.

ABSTRACT This paper generalizes the technique of spatial power combining to modulated signals and applies it to effectively strengthen or deny communications and navigation services in desired area. The system and mathematical model of coherent combining for direct-sequence spread spectrum (DSSS) signals are established. By using the method of transmitting delay precompensation and coherent combination, the coherent energy level after de-spreading at the receiving scales is the square of the number of nodes rather than being additive. Thus, the energy coherence is proposed to analyze the interference and superposition effects in the focusing area rather than the commonly used performance metric of front-end energy analysis. Then, the influences of beam pointing error and clock phase error of the sparse array on coherent combining are studied by theoretical and numerical analysis. The results show that by controlling the array error within a certain allowable range, the proposed method can achieve a precise projection of coherent energy. More specifically, we demonstrate that with further improvements in synchronization and pointing accuracy, the actual distribution of the focal spot and effective interference spots can be precisely manipulated.

INDEX TERMS DSSS signals, spatial power combining, sparse array, synchronization, pointing error.

I. INTRODUCTION

The available transmitted power is constrained by the power limits of microwave devices, while spatial power combining obtains higher energy efficiency and is not subject to this constraint [1]. Because spatial power combining differs in that the energy of all the antenna units is superimposed in the process of spatial propagation. The electromagnetic beam can be formed such that it points in a certain direction, and thus, energy focusing can be realized in the far field intersection region by using the cross beam of the sparse array. Moreover, the spatially combined signal is more conducive to conceal itself, in that the transmitting energy from a single array element is not high enough to be detected by anti-interference and anti-radiation countermeasures. So the Defense Advanced Research projects Agency (DARPA) proposed to apply this technology to precision electronic warfare (PREW) scenarios [2] and Collaborative Operations in Denied Environments (CODE), yielding significant increases in detection and communication range or a denial of quality of service (QoS) [3].

The associate editor coordinating the review of this article and approving it for publication was Zilong Liu.

To the best of our knowledge, the research on spatial power combining with sparse arrays mainly lies in the following three aspects: design and optimization of antenna array patterns for beam shaping and target regions [4]–[7], studies on the effect of far field energy delivery and its combining efficiency [8], [9], and the spatial energy distribution in the near field, which motivates the optimal allocating problem of jamming resources (JRA) [10]–[12]. As for the signal pattern, recent works on spatial power combining are restricted to pulse waveform, sinusoidal signal [8], [13], [14] or taking the broadband signal as a superposition of several single frequency signals [15], [16]. However, no modulated signals have been studied. Therefore, the application of spatial power combining in specific practical systems is still limited to some extent. Spread spectrum signals are widely used in the field of digital communication, increasing both system reliability and communication capacity. Besides the large number of applications in communication systems, spread spectrum signals are also used to obtain accurate range and range rate measurements in radar and navigation. Therefore, when the service of the above-mentioned systems in desired area needs to be strengthened or denied, each array element transmits signal by adopting the same modulation mode,

pseudorandom pattern and other signal parameters, so as to obtain equivalent spreading gain and combined power.

In this paper, we focus on the spatial power combining of a pseudonoise (PN) spread spectrum signal, which is a class of spread spectrum modulations. Specifically, we analyze the spatial energy distribution and focusing characteristic obtained by a sparse array. Rather than the conventional analysis of coherent energy projection by superposing the power or amplitude of simple signals such as single frequency signals or pulse waveforms, the coded spread spectrum signals are bandwidth expanded and thus increase the complexity of the analysis. Concretely, the effect of the combined signals on the target receiver is not only related to the far-field power distribution but also to detection, de-spread and the other signal processing involved at the receiving end. In addition, previous works in spatial power that have combined using sparse arrays are ideally realized, and the error factors of actual transmitting arrays such as the beam pointing accuracy and clock oscillator performance are rarely borne out in simulation and experiments.

The remainder of this paper is structured as follows. Section II describes the spatial power combining model of DSSS signals by using sparse arrays, which includes the system model in Subsection II-A, the proposed method of transmitting delay precompensation and coherent combination in Subsection II-B, and the simulation demonstration in Subsection II-C. Detailed analysis of the node synchronization error and pointing error are shown in Section III and Section IV, respectively. Both theoretical analysis and numerical results are provided to demonstrate the effectiveness of projecting sufficient coherent energy towards the desired area. Concluding remarks are given in Section V.

II. PROBLEM FORMULATION

A. SYSTEM MODEL

The spatial power combination based on sparse array is obtained by arranging array elements (transmitting nodes), which are spaced larger than the wavelength. In order to achieve as much combined signals' power as possible in space and precisely bring them to a specific target area, the following conditions have to be satisfied:

(a) Each node transmits waveform at the same frequency and fixed phase difference.

(b) Each node has synchronized clocks, enabling the signal from each node to be aligned at the desired location [2].

(c) Each node adopts the same polarization mode and antenna beam directivity at the target receiver. But when the polarization of each antenna is different at the target receiver, the coherent energy enhancement can be reduced up to 50% [17], which needs to be analyzed according to the specific antenna geometry and configuration [18].

In this paper, we take the wideband signal modulated by spread spectrum as a typical signal for analysis including the superposed and interfered far-field energy in the area of interest (AOI). The block diagram shown in Fig. 1 illustrates

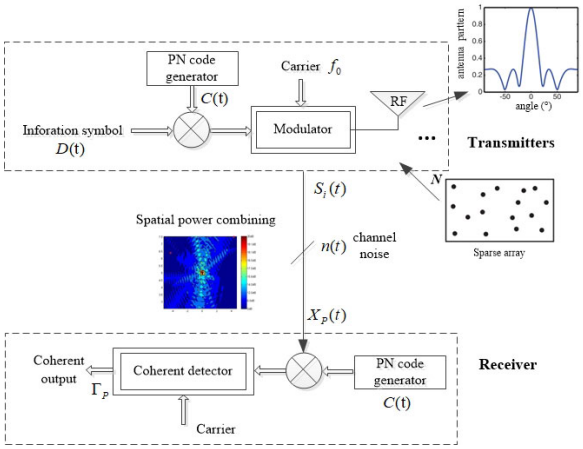

FIGURE 1. Scheme of the spread spectrum system and its spatial power combining model.

the basic elements of a spread spectrum system with two identical pseudorandom pattern generators at the transmitting and the receiving ends. The generators generate a PN binary-valued sequence that is impressed on the transmitted signal at the modulator and removed from the received signal at the demodulator. Therefore, we need to consider the modulation and demodulation when analyzing the spatial combining effect of spread spectrum modulated signals. Besides, the RF front-end and space channel are also elements of the spatial power combining system. Each spread spectrum signal from the sparse array is transmitted separately and combined in spatial channel to project energy into the target region.

Generally, the family of spread spectrum signaling schemes includes PN, frequency-hopped (FH) and linear frequency modulation (LFM) [19]. The PN sequence generated at the modulator is used in conjunction with PSK (Binary Phase Shift Keying) modulation to shift the phase of the PSK signal pseudorandomly. The resulting modulated signal is called a direct sequence (DS) or a pseudonoise spread spectrum signal, which is widely used in the IEEE 802.11 standard, satellite communications, navigation, etc. Thus, in this paper, the spatial power combining technique is generalized to the case of modulated signals and utilized to combine direct sequence spread spectrum (DSSS) signals during propagation of electromagnetic waves after transmitting.

B. COHERENT COMBINING OF DS-BPSK SIGNALS

Following the above system model, the scenario that Binary Phase Shift Keying (BPSK) signal under a certain level of additive white Gaussian noise (AWGN) is considered for two reasons: On the one hand, BPSK modulation is a typical modulation schemes for DSSS systems, from which the rest of the digital phase modulated DSSS signal can be deduced. On the other hand, nonlinear procedures are potentially richer but are also generally more difficult to theoretically tackle. Assume that each transmitter is arbitrarily located on N-nodes in an ad hoc sparse array in which all antennas transmit the

same DS-BPSK signals with different phase shifts and time delays as follows:

$$S_i(t) = A_i D_i(t - T_{id}) C(t - \tau_i - T_{id}) cos(2\pi f_0 t + \varphi_i). \quad (1)$$

where A_i denotes the signal amplitude for $i = 1, 2, \ldots N$ and N denotes the number of nodes. For ease of analysis, suppose that all transmitters have the same excitation amplitude, namely, $A_1 = A_2 = \cdots = A_N = A$. $D_i(t) \in \{+1, -1\}$ denotes the information symbol transmitted at time t. The PN chips $C(t) \in \{+1, -1\}$ are generated by the identical PN generator employed at each transmission array, which only differ in the initial time delay τ_i and propagation time T_{id} from the *ith* transmitter to the center of the AOI. In (1), f_i is the carrier frequency of the transmitted signal, which can be expressed as $f_i = f_0 + \Delta f_i$ with f_0 denoting the nominal frequency and Δf_i denoting the frequency difference. Thus, under low second-order dynamics, we ignore the effect of the frequency variation and include the fixed frequency difference in the signal phase φ_i and rewrite it as $\varphi_i = 2\pi \Delta f_i + \varphi_i'$, where φ_i' is the initial carrier phase controlled by the transmitting arrays.

Due to the relation between the width of information symbol and the period of the PN-code, DSSS signals can be subdivided into two categories: short code and long code. Here, we are mainly concerned with the case when the symbol width is larger than one PN-code period, which means that the information data are slowly varying and can be assumed to be invariant during our analysis interval. For example, for DSSS signals used in navigation systems, information symbols do not affect the receiver's front-end detection and acquisition process. Therefore, it is reasonable to assume that each node transfers identical information symbols $D_i(t) = 1$ during this period. When no synchronization error exists between dispersed nodes, we have $\varphi_1 = \varphi_2 = \cdots = \varphi_N$. After spatial combination, the transmitted DS-BPSK signals at either location $\mathbf{r}$ can be expressed as:

$$\begin{aligned} X(t) &= S(t) + \xi(t) \\ &= \sum_{i=1}^{N} S_i(t) + \xi(t) \\ &= \frac{A}{\|\mathbf{r_i} - \mathbf{r}\|^2} \cos(2\pi f_o t + \varphi) \sum_{i=1}^{N} C(t - \tau_i - T_{id}) + \xi(t) \end{aligned} \quad (2)$$

where $\frac{1}{\|\mathbf{r_i} - \mathbf{r}\|^2}$ is the propagation attenuation and $\|\cdot\|$ is the Euclidean norm. $\xi(t)$ is the additive noise which is independent of signals. In a DSSS system, the receiver first removes the component at $2\pi f_o$ and then removes the PN modulation by correlating with the same periodic sequence. Therefore, the uncorrelated signal can only reduce the signal to noise ratio (SNR) before demodulation but cannot be detected after demodulation. Therefore, the commonly used receiver front-end energy analysis is not enough for the spread spectrum signal in which de-spread, detection and other postprocessing issues are not considered.

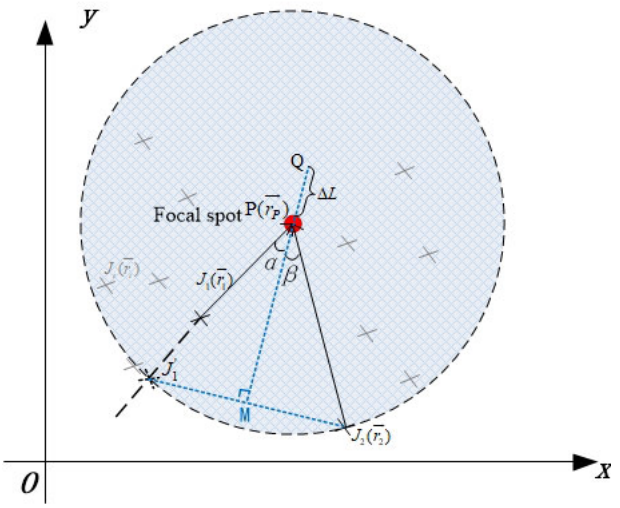

FIGURE 2. Spatial power combination in the focusing region by using sparse arrays.

Consider the scenario shown in Fig. 2. The sparse array is randomly located (as marked by the '×' in Fig. 2), and the transmitting signal is in the direction of $\|\mathbf{r}_i - \mathbf{r}_P\|$ where P is the desired focal spot.

To accurately project enough coherent energy at the focal spot P, theoretically, the PN-code sequence in (2) should be exactly overlapping when it propagates to location P. Thus, we can precompensate the code-delays of the transmitting array by adjusting the relative time delays as below:

$$\begin{aligned} C(t - \tau_1 - T_{1d}) &= C(t - \tau_2 - T_{2d}) = \ldots \\ &= C(t - \tau_N - T_{Nd}) \triangleq C(t - \Delta t) \end{aligned} \quad (3)$$

Suppose T_{code} is the period of the PN-code sequence. Taking the two nodes J_1 and J_2 in Fig. 1 as an example, the relation between τ_1 and τ_2 should satisfy the following condition:

$$\tau_1 - \tau_2 = T_{2d} - T_{1d} = \mathrm{mod}(|PJ_1| - |PJ_2|, T_{code} \times c)/c \quad (4)$$

where mod$(\cdot)$ denotes modular arithmetic and c is the speed of light. In fact, after precompensating the code delay by the above formula, node J_1 is mapped to the virtual point J_1', which is co-circular with node J_2 in Fig. 2. For simplicity, let us consider the case when the distances between each node and the preset focal spot are approximately equal, that is, $\|\mathbf{r}_1 - \mathbf{r}_P\| \approx \|\mathbf{r}_2 - \mathbf{r}_P\| \approx \cdots \approx \|\mathbf{r}_N - \mathbf{r}_P\| = \gamma$. Then, we have

$$X_P(t) = \frac{N \cdot A}{\gamma} \cos(2\pi f_o t + \varphi) C(t - \Delta t) + \xi(t) \quad (5)$$

For the receiving end of the DSSS system, the receiver removes the carrier component and correlates the received baseband signal with the PN sequence [20] in order to detect spatially combined signals. The received noise $\xi(t)$ is white, gaussian, centered, and uncorrelated with the signal. Thus,

the correlation function of the local PN sequence and the baseband PN-code at the receiving end is defined as follows:

$$R_P(\eta) = \frac{N \cdot A}{\gamma} \int_0^{MT_c} C(t - \Delta t + \eta T_c) C(t) dt \tag{6}$$

where T_c is the chip period, M is the number of symbols to be integrated with $M \geq T_{code}/T_c$, Δt denotes the relative PN-code time offset of the received signal, and ηT_c is the phase lag between the local PN-code and the received PN-code at the initial time of detection.

Here, $R_P(\eta)$ denotes a random variable related to the phase shifts at the beginning of detection. It is necessary to remark here that for the receiving end of the DSSS system, a typical detector is based on the second order moment of the estimated correlation, $\Gamma(\eta) = |R_P(\eta)|^2$ [19], [20]. Inspired by this detector, we define the average value of the correlation function $E\left[\left|R_p(\eta)\right|^2\right]$ as the energy coherence at focal spot P. This enables us to quantify the array gains after spatial combination. In this way, we formulate the DSSS spatial energy combining problem. Assuming $C_0(m) = C(mT_c)$, we obtain:

$$\begin{aligned} &E\left[\left|R_p(\eta)\right|^2\right] \\ &= \frac{N \cdot A}{\gamma} E\left[\left|\int_0^{M \cdot T_c} C(t - \Delta t + \eta \cdot T_c) C^*(t) dt\right|^2\right] \\ &= \frac{N^2 \cdot A^2}{\gamma^2} \cdot T_c^2 \cdot E\left[\left|\sum_{j=0}^{M-1} C_0(m - \Delta m + \eta) C_0^*(m)\right|^2\right] \\ &= \frac{N^2 \cdot A^2}{\gamma^2} \cdot T_c^2 \cdot M^2 \end{aligned} \tag{7}$$

Let $R_0(\tau) \overset{def}{=} E\left[C_0(m - \tau) C_0^*(m)\right]$ be the normalized PN-code correlation function. Generally, the autocorrelation function $R_0(\tau)$ of the PN sequences is characterized as

$$R_0(\tau) = \begin{cases} 1 - |\tau|, & |\tau| < 1 \\ 0, & |\tau| \geq 1 \end{cases} \tag{8}$$

Hence, $E\left[\left|R_p(\eta)\right|^2\right] \approx \frac{N^2 \cdot A^2 \cdot M^2 \cdot T_c^2}{\gamma^2}$ is the maximum of the spatial coherent energy projected at spot P, provided that $\eta - \Delta m \in (-1, 1)$, i.e., $\eta T_c - \Delta t \in (-T_c, T_c)$. Compared with noncombining and incoherent far field signal power, the coherent energy increases approximately N^2 times. We can denote the enhancement of the energy coherence values at the P-point in the form of dB:

$$\begin{aligned} \rho_{\max} &\approx 10 \cdot \lg\left(\frac{N \cdot A \cdot M \cdot T_c}{\gamma} \Big/ \frac{A \cdot M \cdot T_c}{\|\mathbf{r}_i - \mathbf{r}_P\|}\right)^2 \\ &\approx 20 \lg N(dB), \quad i = 1, 2, \ldots N \end{aligned} \tag{9}$$

Next, we analyze the energy coherence between the spatially combined transmission signal and the receiving end at an arbitrary spot, Z, other than the tightly focused spot P. Similar to (5), energy coherence at spot Z can be expressed as:

$$\begin{aligned} X_Z(t) = A \sum_{i=1}^{N} \frac{1}{\|\mathbf{r}_i - \mathbf{r}\|} C(t - \Delta t - (|PJ_i| - |ZJ_i|)/c) \\ \cdot \cos(2\pi f_o t + \varphi) + \xi(t) \end{aligned} \tag{10}$$

where $|PJ_i|$ denotes the distance from the node in the sparse array to spot P and $|ZJ_i|$ is the distance to any spot Z. Similarly, the receiving end of Z first removes the carrier and then applies the sliding correlation method to calculate the correlation function as below:

$$R_Z(\eta) = A \int_0^{MT_c} \sum_{i=1}^{N} \frac{1}{\|\mathbf{r}_i - \mathbf{r}\|} \left[\begin{array}{l} C(t - \Delta t + \eta T_c \\ -\frac{|PJ_i| - |ZJ_i|}{c}) C^*(t) \end{array}\right] dt \tag{11}$$

Based on the above derivation, we have $\eta \approx \Delta m$ when the maximum energy coherence is formed at the focal spot; thus,

$$\begin{aligned} &E\left[|R_Z(\eta)|^2\right] \\ &= A \cdot T_c \left| \sum_{j=0}^{M-1} E\left\{ \sum_{i=1}^{N} \left[\begin{array}{l} \frac{1}{\|\mathbf{r}_i - \mathbf{r}\|} C_0^*(m) \cdot C_0(m - \Delta m \\ +\eta - (|PJ_i| - |ZJ_i|)/\lambda_c)) \end{array} \right] \right\} \right|^2 \\ &\approx A \cdot T_c \left| \sum_{j=0}^{M-1} E\left\{ \sum_{i=1}^{N} \left[\begin{array}{l} \frac{1}{\|r_i - r\|} C_0^*(m) \cdot C_0(m \\ -(|PJ_i| - |ZJ_i|)/\lambda_c)) \end{array} \right] \right\} \right|^2 \end{aligned} \tag{12}$$

where $\lambda_c = c \cdot T_c$ denotes the wavelength corresponding to the length of a PN-code chip (i.e., the 1 MHz code rate corresponds to a distance length of 300 m). The energy coherence of the Z point in (12) depends mainly on $\sum_{i=1}^{N} C_0(m - (|PJ_i| - |ZJ_i|)/\lambda_c))$. Because the pseudorandom sequence $C_0(m)$ is periodic with a period equal to T_{code}/T_c, the spatial signals propagated from two arbitrary nodes J_i and J_j will be perfectly superposed if and only if the following formula is satisfied

$$(|PJ_i| - |ZJ_i|) - (|PJ_j| - |ZJ_j|) = n \cdot T_{code} \cdot c (n \in \mathbf{Z}) \tag{13}$$

Otherwise, the signals cannot be combined due to the noise-like characteristics of the pseudorandom sequence.

As illustrated in Fig. 2, after precompensating the code delays, the midperpendicular formed by J_1' and J_2 is the direction in which the energy is in phase. The two signals in the direction of r_1 and r_2 are superimposed in phase at the preset focus P. Then, for the other energy "consistent point" [16] Q adjacent to P, we have

$$\frac{\Delta L \cdot \cos(\alpha) - \Delta L \cdot \cos(\beta)}{T_c \cdot c} = \pm 1 \tag{14}$$

Hence, the energy "consistent point" distributes equally spaced with the period of PN code, and its spacing is $\Delta L = \left|\frac{T_c \cdot c}{\cos(\alpha) - \cos(\beta)}\right|$. When the PN sequences from $k (2 < k < N)$ transmitters are superimposed in phase at Z, a constructive interference effect is formed, and there is also destructive

interference due to the randomness of the PN-code. Therefore, the ''interference effect'' of the energy coherence is presented in the focusing area, which will be simulated and analyzed in subsection II-C.

C. SIMULATION ANALYSIS OF COHERENT COMBINING BY USING SPARSE ARRAYS

When a sparse array consists of multiple nodes that are arbitrarily dispersed, it is difficult to provide an arithmetic formulation to express the distribution characteristics of the combined energy at the focal spot and its neighborhood, while the simulation analysis must ensure that the energy distribution in space is represented without distortion. Therefore, according to the spatial Nyquist sampling law, the simulated spatial sampling interval Δl in the focusing direction should satisfy the following upper bound criterion:

$$\Delta l \leq \min\left\{\frac{1}{2}\Delta L,\ \forall\alpha,\beta\in[0,2\pi)\right\} = \frac{T_c\cdot c}{4} \qquad (15)$$

where $T_c \cdot c$ denotes the spatial distance corresponding to one PN chip. Suppose the grid scale Δx of the x-axis direction is equal to the grid scale Δy of the y-axis direction; then, numerical simulations of the two-dimensional space are done with the condition $\Delta x = \Delta y \leq \Delta l/\sqrt{2} = \sqrt{2}T_c \cdot c/8$. Similarly, the extended three-dimensional simulation can also be done with $\Delta x = \Delta y = \Delta z \leq \sqrt{3}T_c \cdot c/12$ in which Δx, Δy and Δz are grid scales in the x, y, and z axes, respectively. The rest of this subsection presents two-dimensional simulations carried out with the focused spot at a desired location [0 km,5 km]. Each transmitter poses a sinc-pattern antenna with a beam width of 40^o and a horizontal polarization (parallel to the flat surface). The polarization direction of each transmitter is consistent and completely in phase at the target point. The PN-code is an m-sequence generated by a 12-bit register, and the PN-code rate is $1/T_c = 1MHz$ with a period of 1 ms. The receiving end de-spreads the DSSS signal by using the same PN sequence as the transmitting end. We take the second-order moment of the correlation function as the detector [20] and an ideal filter with a bandwidth of $20MHz$ as the front-end filtering. We set the grid scale to 50 m, which is less than the threshold of the two-dimensional grid scale. The transmission array is composed of $N = 2$ and $N = 10$ transmitters. For spatial power combining with DSSS signals, we can see the enhancement of energy coherence values after the spatial combining from the simulation results shown in Figs. 3-4. We use the color scale shown in the legend to represent the energy coherence enhancements (the unit is dB) in the region.

As shown in Fig. 3, the transmitters are randomly located on the horizontal axis, while the white asterisk indicates the desired focal spot P, i.e., the small spot with the maximum enhancement in energy coherence. The focused energy from $N = 2$ transmitters in Fig. 3(a) is 6 dB (four times) stronger than the energy coherence from a single transmitter, while for the $N = 10$ transmitters in Fig. 3(b), this can be enhanced by 20 dB (100 times). The tightly focused spot and its neighborhood are approximately 300 m in diameter,

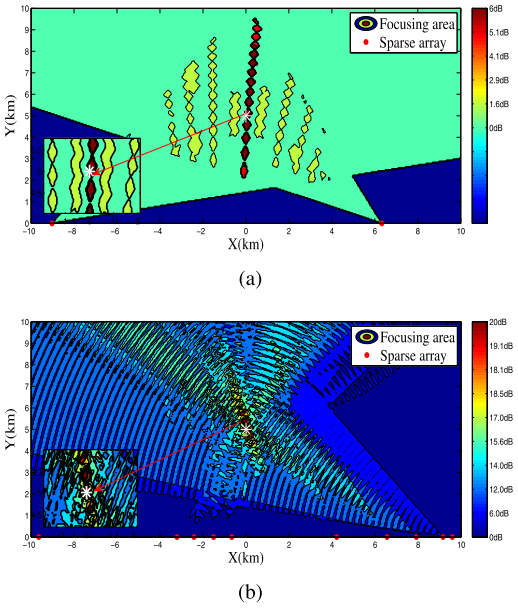

FIGURE 3. Coherent combining simulation by using a linearly dispersed sparse array: (a) $N = 2$, (b) $N = 10$.

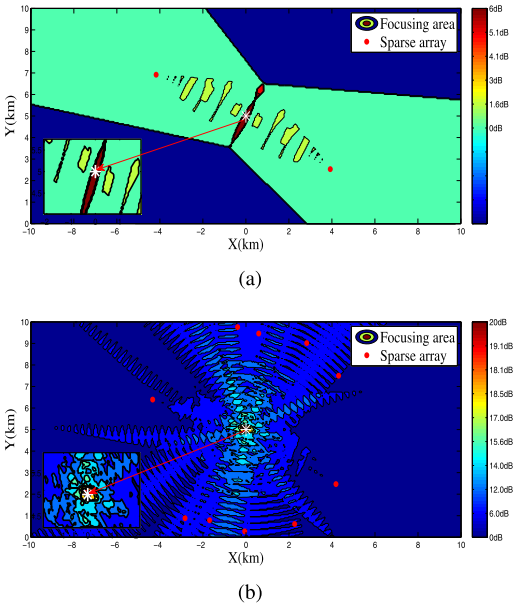

FIGURE 4. Coherent combining simulation by using a sparse array in the annular region: (a) $N = 2$, (b) $N = 10$.

which is determined by the width of a single PN-code chip. In addition, Figs. (a) and (b) show an ''interference'' effect in the entire region besides P, and the distribution of consistent interference points conforms to equation (13) and (14). The interference fringe region corresponding to the adjacent transmitters has stronger coherent energy. Conversely, since the nodes are most sparsely distributed on the left side, the energy coherence increases by less than 3 dB within the radiation range (upper right in Fig. (b)). The coherent energy distribution obtained using a sparse array setting in an annular region

is shown in Fig. 4. The radius is 4.5-5 km from the sparse array to the desired focal spot, and the other simulation setup is the same as above.

As for the interference effect, similar conclusions follow as for the linear distribution array. In particular, the focusing area is more concentrated and the energy defocusing area is less than in the linear array. Thus, the specific array scheme should be determined according to the spatial energy distribution. The denser the array, the stronger is the corresponding interference fringe energy and vice versa. From the above simulation results, we demonstrate that by precompensating the code delay of the transmitting signals and combining them in space, the transmitted energy is successfully focused on the desired spot, and the maximum gain of $20\cdot\lg N(dB)(N^2\text{times})$ can be obtained.

III. SYNCHRONIZATION ERROR ANALYSIS

The PREW report released by DARPA points out that the clock synchronization and accurate pointing provide technological foundation for spatial power combination. However, the synchronization error and beam pointing error still exist, so the previous optimal energy combination can not be realized in the actual situation. In order to verify the feasibility and effectiveness of the proposed method in nonideal cases, the effect of synchronization error on coherent combining DSSS signals is firstly analyzed in this section.

A. PROBLEM REFORMULATION

The spatial power combining system envisions an array of nodes that have synchronized clocks enabling the signal from each node to be aligned so that the array focuses energy at the desired location. In the theoretical and simulation analysis of the previous section, it is assumed that there is no synchronization error between the nodes. However, even if accurate timing devices and techniques are utilized to synchronize dispersed clocks, there are still some errors in the actual sparse array such as the oscillator deviation, time transfer error, device calibration error, etc. Therefore, the spatial combining effect analysis of the modulated signals at microwave frequencies (electromagnetic wave in the frequency range of 300 MHz - 300 GHz) must consider the node synchronization error, which is the objective of this section.

Assuming that the node synchronization error is δt_i, then the spatially combined signal can be reformulated as follows:

$$S(t) = A\sum_{i=1}^{N}\cos[2\pi f_o(t+\delta t_i)+\varphi]C(t+\delta t_i-\tau_i-T_{id}) \tag{16}$$

Assuming that the node clock error is uniformly distributed within the synchronization accuracy equals $\mu(\mu \geq 0)$, namely, $\delta t_i \sim U[-\mu,\mu]$. When $\mu = T_c$, the influence of node synchronization error on the alignment of the PN-code is very small. For example, the PN-code chip period corresponding to 1 MHz code rate is $T_c = 1\mu s$, while the general node synchronization precision is on the order of ns.

TABLE 1. Location of sparse array in the numerical analysis (unit: km).

Nodes No.	1	2	3	4	5	6	7	8	9	10
Horizontal coordinate	3.74	-0.84	-4.75	4.73	4.86	1.81	4.14	3.48	4.06	-3.30
Vertical coordinate	7.63	9.64	3.56	3.71	3.91	0.79	2.22	8.56	2.54	1.38

Thus, the influence of synchronization error on PN-code alignment is negligible. However, it is mainly affected by the phase of the carrier-modulated microwave signals. Since δt_i is a random variable, we analyze the statistical characteristics of the carrier modulated signal after spatial combining.

$$\begin{aligned} &E\left\{A\cdot\sum_{i=1}^{N}\cos[2\pi f_o(t+\delta t_i)+\varphi]\right\} \\ &= A\cdot\sum_{i=1}^{N}\left\{\int_{-\mu}^{\mu}\cos[2\pi f_o(t+\delta t_i)+\varphi]\cdot\frac{1}{2\mu}d\delta t_i\right\} \\ &= A\cdot N\cos(2\pi f_o t+\varphi)\cdot Sa(2\pi f_o\mu) \end{aligned} \tag{17}$$

As we know, the above Sa function possesses the following properties: the smaller μ is, the stronger the energy of the combined carrier signal, and if $\mu > \frac{1}{2f_0}$, the array gain of (17) significantly declines. Accordingly, in theory, the efficacy of projecting sufficient coherent energy requires the time synchronization accuracy to be controlled within a half carrier period. The real-time clock phase error stabilized by recent synchronization techniques is kept at the order of 0.05 ns and 0.5 ns within a day, which provides a theoretical basis for the subnanosecond time demand of signal frequencies below 1 GHz. However, a clock jump of ns order still exists [22], [23], and the greater the number of nodes, the more complex is the impact of synchronization errors. In the following, we will further analyze this by using simulation experiments.

B. NUMERICAL RESULTS

This subsection presents the outcomes of numerical verification efforts. A practical scenario involving different node synchronization errors is presented to demonstrate the energy coherence, field distribution characteristics and effective interference points in the focusing area.

Based on the theoretical analysis in the previous subsection, the node clock phase error is set to the following different synchronization accuracies: $\mu = 0$ (error-free), $\mu = \frac{1}{8f_0}$, $\mu > \frac{1}{4f_0}$ and $\mu = \frac{1}{2f_0}$. The other parameter settings are the same as in Fig. 4(b).

Take as an example the ten randomly located nodes whose locations are listed in Table 1 with a grid scale of 0.1 m. The energy distribution of the spatially combined DSSS signals at microwave frequencies is analyzed by two-dimensional simulation. As shown in Fig. 5, the energy coherence distribution also presents an interference phenomenon in the focusing area. Due to the high frequency and the large number of node signals, the signal interference effects between nodes overlap with each other. Thus, there exists in-phase superpositions

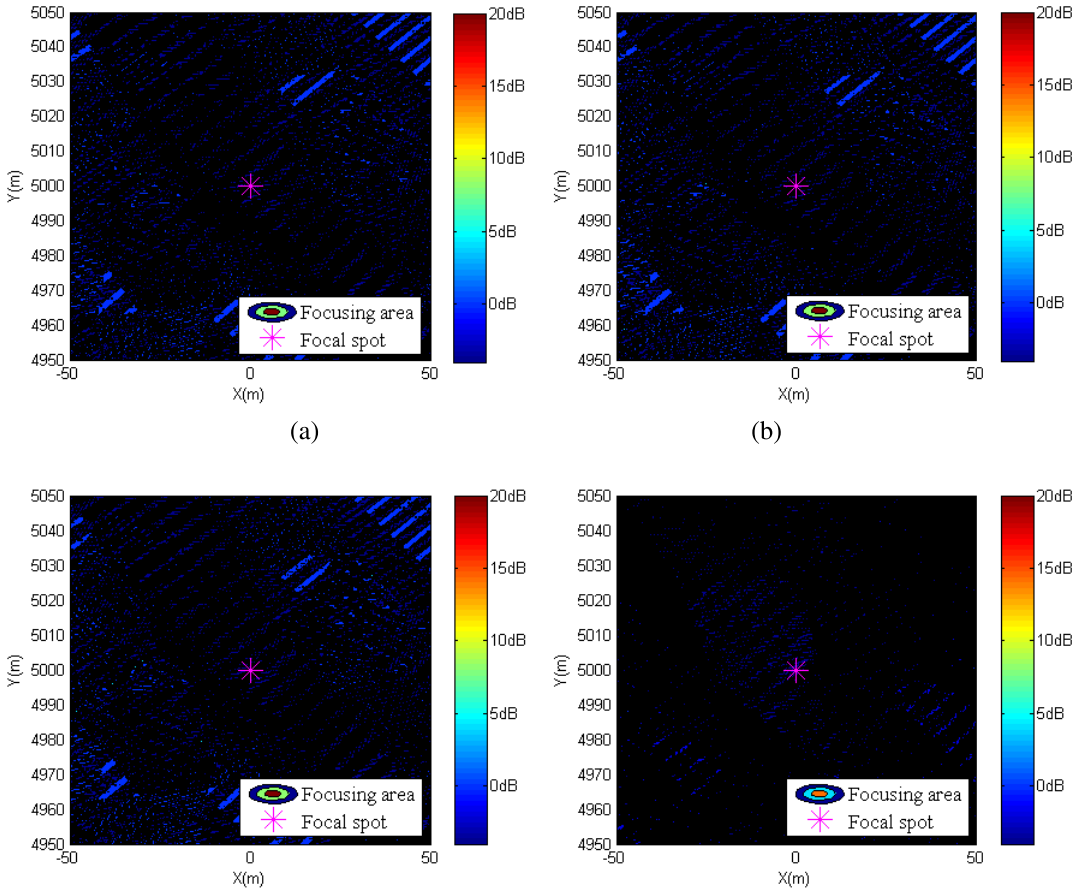

FIGURE 5. Distribution of energy coherence in the focusing area ($100m \times 100m$), $f_0 = 300MHz$: (a) $\mu = 0$; (b) $\mu = \frac{1}{8f_0}$; (c) $\mu = \frac{1}{4f_0}$; (d) $\mu = \frac{1}{2f_0}$.

of partial arrays other than the preset focus point, P. At the focal spot P and its neighborhood, the region whose coherent energy enhancement ρ satisfies $\rho \geq {\rho_{\max}}/{Th}$ is regarded as the effective interference region (where Th is the threshold set as needed). Assuming $Th = 2$, the effective interference region is extracted, as shown in Fig. 6.

Fig. 6 shows the distribution of the effective interference region. It can be clearly seen that the node synchronization error has a varying impact on the energy interference in the focusing area. Considering the error δt_i within the range of $\pm\frac{1}{8}$ and $\pm\frac{1}{4}$ carrier period (as shown in Fig. 6(b) and (c)), there is only a difference in position from the theoretical distribution in Fig. 6(a). However, in the case of δt_i distributing in $[-\frac{1}{2f_0}, \frac{1}{2f_0}]$, a small amount of energy can be effectively focused at the desired location and is defocused in the upper neighborhood. The aforementioned theoretical conclusions in Subsection 3.2 are therefore confirmed. Because the effective interference mainly concentrates near the focal spot P, we observe the related energy projection of the P point by narrowing the analysis window in Fig. 5. Fig. 7 shows the coherent energy distribution of the focal neighborhood in the 10^2m^2 region, which is conducted under the same conditions and grid-scale as in Fig. 5. As shown in Fig. 7(a), the spatial energy coherence also presents an interference phenomenon in the analysis window forming a narrow effective interference region around the preset focusing spot P (marked with the red frame line in the figure and the local magnification above it). The interference ripple width is approximately 5 m, and the energy is gradually focused at the center point P in the effective interference region.

As shown in Fig. 7(b), with the range of synchronization error increasing to $\pm\frac{1}{8f_0}$ carrier period, the position of the focal spot is unchanged, and the maximum coherent energy after spatial combination is estimated to be increased by 19.74 dB. When the synchronization error continues to increase to the range of$\pm\frac{1}{4f_0}$, the focal spot has shifted (in the upper left frame line in Fig. (c)) to $\left[P_x - 4.2, P_y + 2\right]$ $(unit : m)$ with a maximum energy coherence of 19.48 dB, while at the original preset point P, the energy coherence is only increased by 14.96 dB. Compared to the error-free situation, the larger the synchronization error, the greater is the difference in the distribution of spatial

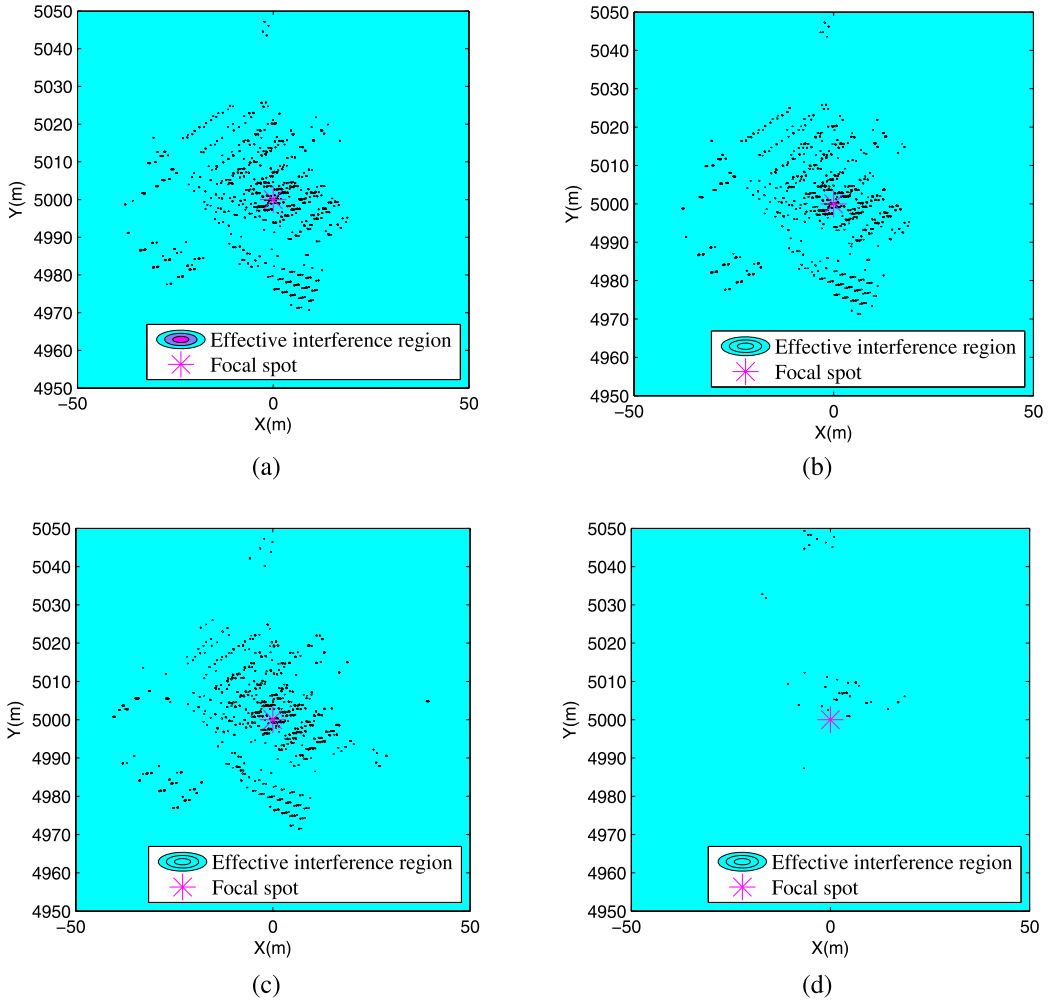

FIGURE 6. Image of the effective interference region (100m × 100m): (a) $\mu = 0$; (b) $\mu = \frac{1}{8f_0}$; (c) $\mu = \frac{1}{4f_0}$; (d) $\mu = \frac{1}{2f_0}$.

energy. And the actual focus will deviate from the desired position, enabling to deliver enough signal power. Especially when the synchronization error reaches half a carrier cycle (as shown in Fig. 7(d)), the energy combining effects of the focusing area are significantly reduced, the focal spot is greatly shifted, and the effective interference area is only 5% of the other cases. To further analyze the influence of node synchronization error on the focusing area and the actual coherence energy of spot P, we have carried out several sets of simulation experiments. Due to space limitations, we cannot show the results of all the distributions. The statistical results are given in tabular form below.

It can be seen from the above table that when the node synchronization error between sparse arrays is controlled within $\pm\frac{3}{16f_0}$, the energy can be accurately projected at the preset focal spot losing no more than 20% of the total energy. Due to the pseudorandomness of the PN signals, the actual energy at spot P is also to some extent randomly distributed. However, as the error increases, the reduction in synchronization accuracy tends to result in more position uncertainty and greater coherent energy loss at the actual focal spot. In short, to project energy from a sparse array to form a tightly focused spot on a desired location, the node synchronization error must be within a limited accuracy range. Considering the

TABLE 2. The effect of synchronization error on the spatial power combining, $N = 10$.

Synchronization accuracy	$\rho_{\max}$	Energy enhancement at spot P	Actual focal position(m)	
			Horizontal coordinate	Vertical coordinate
$\pm\frac{1}{16f_0}$	19.8dB	19.8dB	P_x	P_y
$\pm\frac{1}{8f_0}$	19.6dB	19.4dB	P_x	P_y
$\pm\frac{3}{16f_0}$	19.6dB	18.4dB	P_x	$P_y + 0.1$
$\pm\frac{1}{4f_0}$	19.4dB	15.0dB	$P_x + 3$	$P_y + 2$
$\pm\frac{5}{16f_0}$	17.2dB	10.0 dB	$P_x - 1.2$	$P_y + 3.7$
$\pm\frac{3}{8f_0}$	16.8dB	16.4dB	$P_x - 4.2$	$P_y + 1.9$
$\pm\frac{7}{16f_0}$	15.8dB	5.6dB	$P_x - 1.7$	$P_y + 4.7$
$\pm\frac{1}{2f_0}$	15.6dB	7.8 dB	$P_x - 4.2$	$P_y + 2$

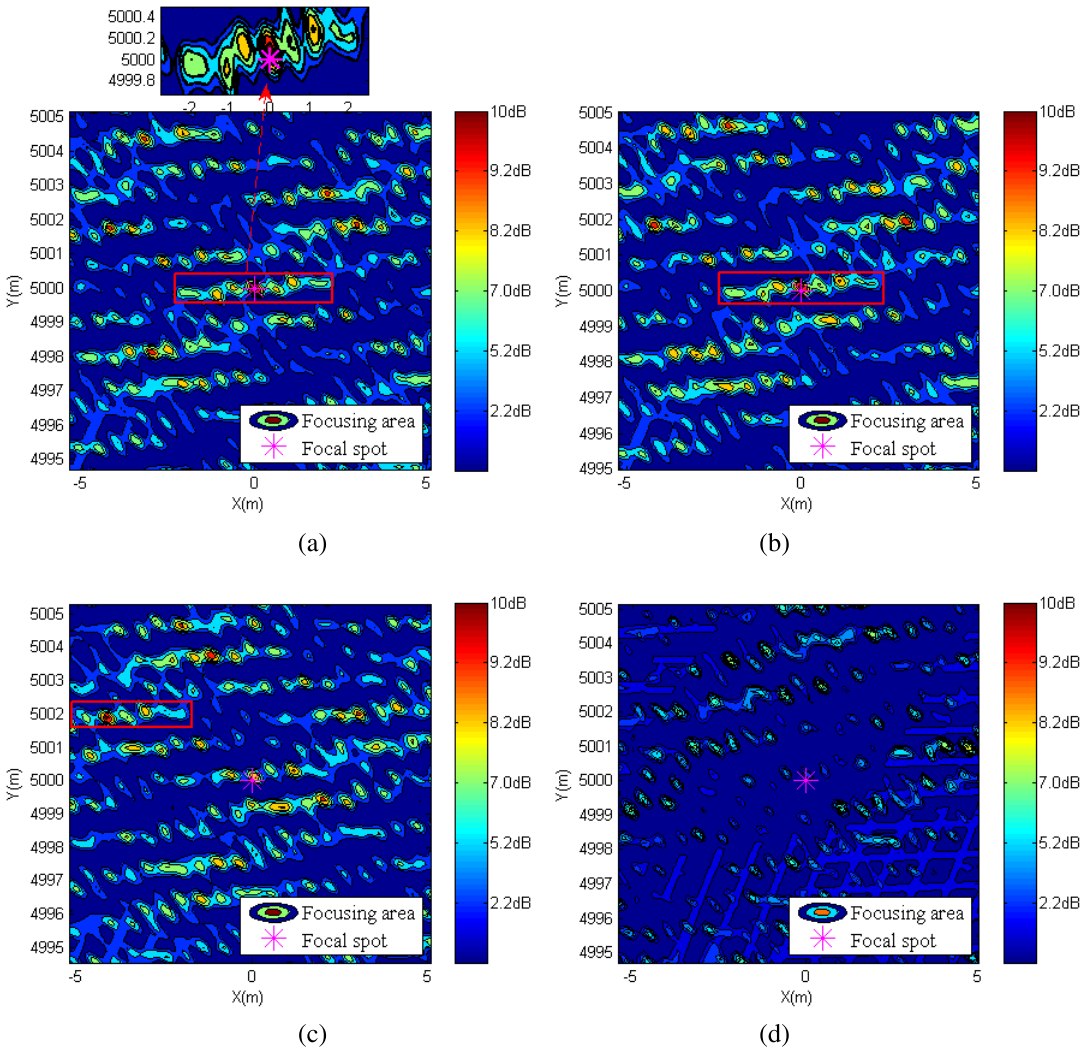

FIGURE 7. Distribution of energy coherence in the focusing area ($10m \times 10m$): (a) $\mu = 0$; (b) $\mu = \frac{1}{8f_0}$; (c) $\mu = \frac{1}{4f_0}$; (d) $\mu = \frac{1}{2f_0}$.

coherence energy enhancement at both the focused spot and its neighborhood, the node synchronization accuracy should be controlled within $\pm\frac{3}{16}$ of the carrier period. When the synchronization error exceeds one-half of the carrier period, the target receiver in desired area would not be effectively denied when the synchronization error exceeds one-half of the carrier period. Or the signal would not reach the desired area when applying to expand the communication or navigation range.

IV. POINTING ERROR ANALYSIS

In the theoretical and simulation analyses of the previous sections, it is assumed that the center of the main lobe of each node's antenna points towards the focal spot. However, apart from the time delay control of signals and oscillator synchronization, accurate pointing is also a key challenge for the spatial power combining technique. The impact of pointing error on coherent energy projection will be analyzed in this section. Increasing the pointing accuracy of each node is one of the factors that improves the efficiency of far field focusing. Reference [3] pointed out that the projection of coherent energy to a small spot (e.g., 10 m average diameter) over long distances (i.e., up to 10 km slant range) is expected to require milliradian level pointing. The definition of beam pointing loss is given in this report. However, no detailed analysis or metric modes are described for this conclusion. In this section, the metric that is being used to determine the impact on focusing effectiveness is the percentage of energy loss relative to the maximum energy coherent gain.

In order to measure the impact of pointing error on focusing effectiveness, another numerical simulation is carried out considering different pointing errors ∂_i, $i = 1, 2, \ldots, N$ $(unit : rad)$ of a sparse array composed of transmitters. Assuming that the pointing errors ∂_i conform to a normal distribution, they are set to the following: $\partial_i = 0$, $\partial_i \sim N(0.001, 0.05)$, $\partial_i \sim N(0.01, 0.05)$ and $\partial_i \sim N(0.1, 0.5)$. We still considered "sinc-patterns" that have side lobes of constant width and varying height to analyze the

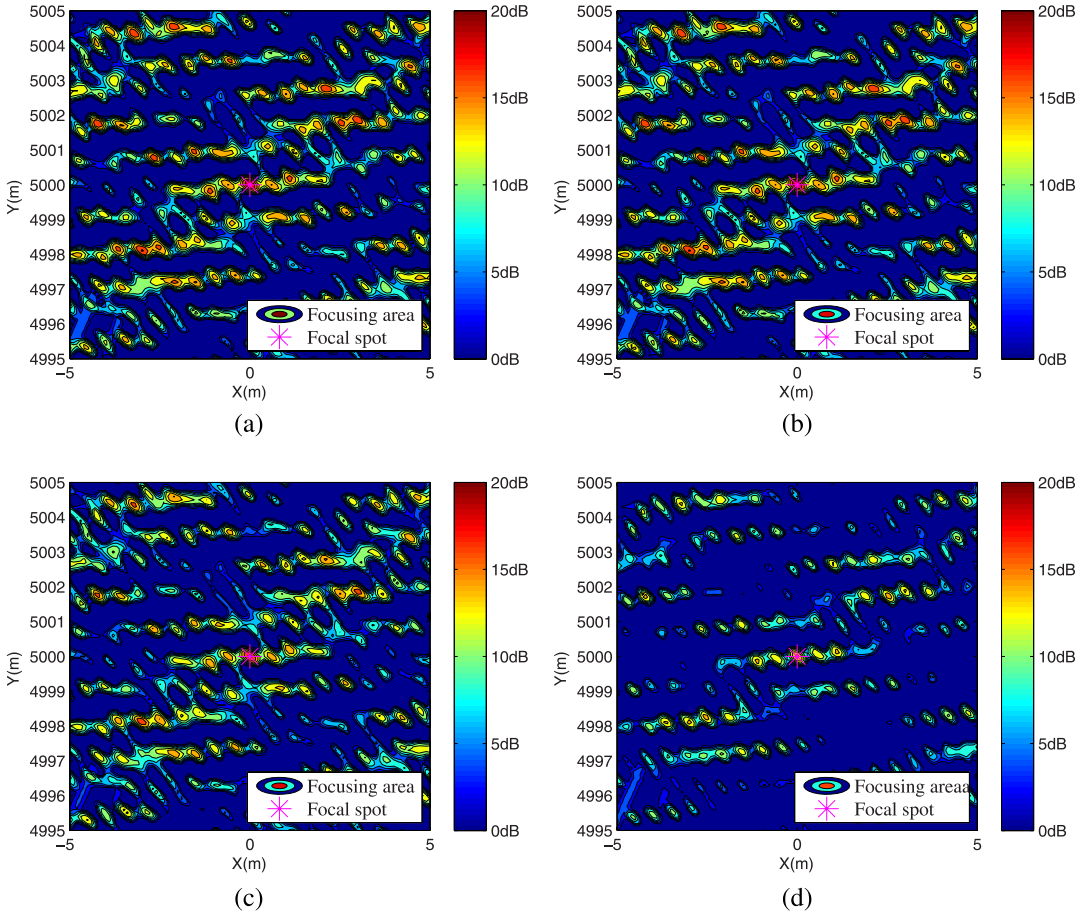

FIGURE 8. Distribution of energy coherence in the focusing area (Distribution of energy coherence in the focusing area ($10m \times 10m$): (a) $\partial_i = 0$; (b) $\partial_i \sim N(0.001, 0.005)$; (c) $\partial_i \sim N(0.01, 0.05)$; (d) $\partial_i \sim N(0.1, 0.5)$.

pattern [23], [24], and the other parameter settings are the same as in the previous numerical example.

The spatial energy distributions for different node pointing errors are shown in Fig. 8. Compared with the ideal case of Fig. 8(a), the different pointing error cases shown in the other figures do not affect the location of the focal spot and the effective interference spots but only affect the array gain, thus resulting in a loss of energy coherence at the focal spot. From the statistical analysis of Fig. 8(b-d), the coherent energy loss is 14.9%, 24.1% and 53.3%. Thus, inaccurate pointing control will inevitably affect the efficiency of spatial power combining. In fact, the pointing error metric is merely the drop in actual array gain, which is independent of the drop in coherent power and the offset of the spatial position due to the clock phase error analyzed in Section III.

V. CONCLUSIONS

Based on the principle of power combining by using sparse array, the coherent combining method of modulated signals is studied. Energy coherence is proposed to analyze the coherent combining effect based on the de-spread output of the receiving end, i.e., not just the input power of the receiver front-end. Then, the results of coherent combining DSSS signals from two or more transmitters are theoretically calculated and numerically simulated in Section II. The results present an ''interference effect'' in the focusing area: the spatial energy constructively interferes when the PN sequences overlap so that the superposition can be realized by precompensating the time offsets between the transmitting array, and then N^2 times gain in the coherent energy can be realized using the proposed method. Moreover, the non-alignment of the transmitting array beams pointing and clock phase of DSSS signals at microwave frequencies cannot be ignored. Numerical simulations in Sections III and IV indicate that 1) the clock phase error results in the defocus of energy at the desired location and the simultaneous decrease in array gains. To realize an effective energy combination in the focusing area and its neighborhood, the node synchronization error of the sparse array should be controlled within half of the carrier period. Then, with the further improvement in synchronization accuracy, the actual energy distribution of the focal spot and the effective interference spots can be precisely manipulated. 2) The effect of beam pointing error on spatial energy combining is only a drop in amplitude but does not affect the position offset of interference spots. This paper is a preliminary exploration to extend the spatial energy

combining technique to modulated signals. It is necessary to further study the controllability of effective interference regions by adjusting the position and formation of the sparse array. The methods and conclusions presented in this paper are the theoretical basis for combining modulated signals in the open space and extending the communication, navigation and jamming range.

REFERENCES

[1] M. P. DeLisio and R. A. York, "Quasi-optical and spatial power combining," *IEEE Trans. Microw. Theory Techn.*, vol. 50, no. 3, pp. 929–936, Mar. 2002.
[2] P. Calhoun, "DARPA emerging technologies," U.S. Air Force Test Pilot School, Edwards, CA, USA, Tech. Rep., 2016.
[3] N. Fox, "Precision electronic warfare (PREW)," Strategic Technol. Office US Defense Adv. Res. Projects Agency, Arlington, VA, USA, Tech. Rep. BAA 09-65, Aug. 2009.
[4] D. Song, W. Wang, Z. Xu, Z. Xiong, and T. Kirubarajan, "Focused energy delivery with protection for precision electronic warfare," *IEEE Trans. Aerosp. Electron. Syst.*, vol. 52, no. 6, pp. 3053–3064, Dec. 2016.
[5] C.-C. Cheng, M. Di Renzo, F. Graziosi, and A. Zappone, "On simultaneous wireless information and power transfer for receive spatial modulation," *IEEE Access*, vol. 5, pp. 23204–23211, 2017.
[6] B. Friedlander, "On transmit beamforming for MIMO radar," *IEEE Trans. Aerosp. Electron. Syst.*, vol. 48, no. 4, pp. 3376–3388, Oct. 2012.
[7] D. Song, W. Wang, Z. Xiong, and Z. Xu, "Waveform diversity based regional energy focusing under ultra-sparse array," *J. Electron. Inf. Technol.*, vol. 36, no. 5, pp. 1082–1087, 2014.
[8] P. Angeletti and G. Toso, "Array antennas with jointly optimized elements positions and dimensions part I: Linear arrays," *IEEE Trans. Antennas Propag.*, vol. 62, no. 4, pp. 1619–1626, Apr. 2014.
[9] A. M. Haimovich, R. S. Blum, and L. J. Cimini, "MIMO radar with widely separated antennas," *IEEE Signal Process. Mag.*, vol. 25, no. 1, pp. 116–129, Jan. 2008.
[10] H. Jiang, Y. Zhang, and H. Xu, "Optimal allocation of cooperative jamming resource based on hybrid quantum-behaved particle swarm optimisation and genetic algorithm," *IET Radar, Sonar Navigat.*, vol. 11, no. 1, pp. 185–192, Jan. 2017.
[11] I. Vizitiu, *Fundamentals of Electronic Warfare*. Bucharest, Romania: Matrix Rom, 2011.
[12] S. Bayram, N. D. Vanli, B. Dulek, I. Sezer, and S. Gezici, "Optimum power allocation for average power constrained Jammers in the presence of non-Gaussian noise," *IEEE Commun. Lett.*, vol. 16, no. 8, pp. 1153–1156, Aug. 2012.
[13] H. Tu, S. Xiao, Z. Yang, and B.-Z. Wang, "Research on the single-frequency super-resolution focusing of micro-structured antenna based on time reversal electromagnetic wave," *Acta Phys. Sinica-Chin. Ed.*, vol. 63, no. 8, Apr. 2014, Art. no. 084102.
[14] Q.-J. Chen, Q.-X. Jiang, F.-L. Zeng, and C.-B. Song, "Single frequency spatial power combining using sparse array based on time reversal of electromagnetic wave," *Acta Phys. Sinica*, vol. 64, no. 20, Oct. 2015, Art. no. 0204101.
[15] L. Gong, "The research of the spatial-temporal focusing in time reversal and its application in wireless communication," M.S. thesis, School Commun. Inf. Eng., Univ. Nanjing, Nanjing, China, May 2015.
[16] Q. Jiang, Q. Chen, L. Fan, and L. Tan, "Interference synthesis of cross beams from sparse array," *High Power Laser Part. Beams*, vol. 28, no. 5, 2016, Art. no. 053201.
[17] T. Lu, "Research on synthesis of sparse volumetric array," Ph.D. dissertation, School Electron. Sci. Eng., Univ. Electron. Sci. Technol. China, Chengdu, China, May 2009.
[18] X. Ren and X. Chen, "Efficiency of microwave power spatial synthesis under random phase shift," *High Power Laser Part. Beams*, vol. 27, no. 8, pp. 1041–1044, 2009.
[19] G. Burel, C. Bouder, and O. Berder, "Detection of direct sequence spread spectrum transmissions without prior knowledge," in *Proc. IEEE Global Telecommun. Conf.*, vol. 1, Nov. 2001, pp. 236–239.
[20] J. G. Proakis and M. Salehi, *Communication Systems Engineering*, vol. 2, 2nd ed. Upper Saddle River, NJ, USA: Prentice-Hall, 1994.
[21] Z. Dai, X. Dai, Q. Zhao, Z. Bao, and C. Li, "Multi-GNSS real-time clock estimation using the dual-thread parallel method," *Adv. Space Res.*, vol. 62, no. 9, pp. 2518–2528, Nov. 2018.
[22] Y. Yao, Y. He, W. Yi, W. Song, C. Cao, and M. Chen, "Method for evaluating real-time GNSS satellite clock offset products," *GPS Solutions*, vol. 21, no. 4, pp. 1417–1425, Oct. 2017.
[23] R. C. Johnson and H. Jasik, *Antenna Engineering Handbook*, vol. 1356. New York, NY, USA: McGraw-Hill, 1984.
[24] W. Zhang and T. Su, "Reference beam pattern design for frequency invariant beamforming based on fast Fourier transform," *Sensors*, vol. 16, no. 10, p. 1554, Oct. 2016.

XIAOFENG OUYANG was born in China, in 1989. She received the bachelor's and master's degrees from the National University of Defense Technology (NUDT), China, in 2011 and 2014, respectively, where she is currently pursuing the Ph.D. degree. Her main research interests include in the areas of digital communication system and satellite navigation system.

FANGLING ZENG was born in China, in 1970. She received the B.Sc., master's, and Ph.D. degrees from the University of Science Technology (USTC), China, in 1996, 1999, and 2002, respectively. She is currently a Professor with the National University of Defense Technology. Her main research interests include satellite navigation system and electronic warfare.

DAQIAN LV was born in China, in 1990. He received the master's degree from the School of Electronic Countermeasures, National University of Defense Technology (NUDT), Hefei, China, in 2016, where he is currently pursuing the doctoral degree. His research interests include in the areas of precise point positioning and time synchronization technique.

WENHAO WANG was born in China, in 1986. He received the master's degree from the School of Electronic Science, National University of Defense Technology (NUDT), Hefei, China, in 2014, where he is currently pursuing the doctoral degree. His research interests include in the areas of data processing.